SCIENTIFIC REPORTS

OPEN

SUBJECT AREAS:
STRUCTURAL PROPERTIES
TWO-DIMENSIONAL MATERIALS

Received
28 October 2013

Accepted
11 February 2014

Published
26 March 2014

Correspondence and requests for materials should be addressed to J.S. (junsun@mail.xjtu.edu.cn) or G.L. (lgsammer@mail.xjtu.edu.cn)

Achieving optimum mechanical performance in metallic nanolayered Cu/X (X = Zr, Cr) micropillars

J. Y. Zhang, J. Li, X. Q. Liang, G. Liu & J. Sun

State Key Laboratory for Mechanical Behavior of Materials, Xi'an Jiaotong University, Xi'an, 710049, P.R. China.

The selection and design of modern high-performance structural engineering materials such as nanostructured metallic multilayers (NMMs) is driven by optimizing combinations of mechanical properties and requirements for predictable and noncatastrophic failure in service. Here, the Cu/X (X = Zr, Cr) nanolayered micropillars with equal layer thickness (h) spanning from 5–125 nm are uniaxially compressed and it is found that these NMMs exhibit a maximum strain hardening capability and simultaneously display a transition from bulk-like to small-volume materials behavior associated with the strength at a critical intrinsic size $h \sim 20$ nm. We develop a deformation mode-map to bridge the gap between the interface characteristics of NMMs and their failure phenomena, which, as shrinking the intrinsic size, transit from localized interface debonding/extrusion to interface shearing. Our findings demonstrate that the optimum robust performance can be achieved in NMMs and provide guidance for their microstructure sensitive design for performance optimization.

A central focus of materials science & engineering has been to discover and understand the important correlations between the properties and performance of materials, their microstructures, and the processing methods required to achieve them–and then to exploit these in the design of engineered components[1,2]. In the future micromechanical devices, the nanostructured metallic multilayers (NMMs) can play a leading role due to their desirable mechanical properties and performance, such as superior strength, relatively high deformability, excellent morphological stability, and great radiation tolerance, making them uniquely multifunctional materials to satisfy special needs[3–8]. NMMs often display intrinsic layer thickness (h)-dependent strengthening and hardening capability and near-theoretical strength at small h[9–14], which is closely related to both the density and the structures/properties of interfaces[15,16]. As the density of interfaces increases (due to smaller h) the strength (σ) as well as the strain hardening capability of NMMs structures becomes increasingly determined by the specific nature and properties of the interfaces, *e.g.* (fully) coherent and semi/incoherent interfaces[17,18]. Experimental, theoretical, and modeling works have demonstrated that plastic deformation including nucleation, multiplication, accumulation, and transmission of dislocations, referred to as interface-mediated plasticity, is strongly connected to characteristics of interface structure *i.e.*, the interfacial dislocation network[19–22]. These processes can render the instability of interface structure, the rotation and/or sliding of interfaces, shearing/crossing of interfaces and twinning, in various nanolayered structures such as FCC/BCC Cu/Nb[10,11] and FCC/FCC Cu/Au[23], which closely correlate with the size-dependent deformation modes of nanolayered micropillars[10,11,24].

In the past decade, the vast majority of uniaxial deformation experiments and computations on small-scale metallic structures (*e.g.* single crystals and nanostructured monolithic thin films) unambiguously demonstrated that at the micron and sub-micron scales, there is a strong "extrinsic size effect" on their robust performance[25–29], which can be described as $\sigma \propto A\phi^{-\alpha}$, where A is a constant, ϕ is sample diameter and α is the power-law exponent ($\alpha \sim 0.5$–0.97 for FCC, $\alpha \sim 0.42$–0.68 for HCP and $\alpha \sim 0.22$–0.48 for BCC crystals)[25–29]. As both the intrinsic (*i.e.*, microstructural) and extrinsic (*i.e.*, sample dimension) sizes play a non-trivial role in the mechanical properties and deformation mechanisms of small-scale structures, it is critical to develop an understanding of their interplay and mutual effects on the mechanical properties and deformation of materials, which in turn guides the microstructure sensitive design for their optimized performance. In this work, we systematically investigated the intrinsic layer thickness (h) and extrinsic sample diameter (ϕ) effects on the mechanical properties and deformation (failure) modes of Cu/Zr NMMs (with large mismatch strain $\delta \sim 11.2\%$) and those of Cu/Cr NMMs (with small mismatch

strain $\delta \sim 2.3\%$) by microcompression methodology to provide deep insights into the associations of internal microstructure-external limitation-performance in small-scale nanolayered micropillars.

Results

Internal features of nanolayered micropillars. The typical TEM images of Cu/X (X = Cr, Zr) NMMs are presented in Fig. 1, from which one can see the modulated layered structure and distinguishable interfaces. The selected area diffraction patterns indicate that the present NMMs show strong Cu (111), Zr (0002) and Cr (110) textures, consistently with the X-ray diffraction patterns. The measured average dislocation spacing (λ) between dislocations with the same Burgers vector $\boldsymbol{b} = a/2[110]$ parallel to the interface is of ~1.7 nm and ~10.2 nm in Cu/Zr and Cu/Cr, respectively. (Misfit dislocations with other Burgers vectors are not considered here.) These values are somewhat smaller than their corresponding theoretical values calculated by $\lambda = b/\delta$, *i.e.*, ~2.3 nm for Cu/Zr and ~11.1 nm for Cu/Cr. The nano-sized grains (d) of Cu, Cr and Zr layers all scale with h. More details can be found in Supplementary Information.

Mechanical response of nanolayered micropillars. Fig. 2(a) and (b) show the typical true stress – strain curves of $\phi = 800$ nm and $h = 10$ nm Cu/Zr pillars, respectively, from which several features can be observed: (i) A gradual transition between elastic and plastic deformation; (ii) after the stress reaches a maximum, gradual softening, which can be attributed to the dislocations annihilation-induced work softening at greater h and shear banding caused geometrical softening at smaller h[10–13,22] occurs until failure ensues; (iii) the strain hardening behavior can be described by Ludwik's equation[30], *i.e.*, $\sigma = K_1 + K_2\varepsilon_p^n$, where K_1 represents the initial yield stress, K_2 is the strengthening coefficient and n is the strain hardening exponent. The values of n determined for the three extrinsic ϕ-sized pillars exhibit the same fashion — n monotonically decreases with reducing h, and are quite close to each other for the pillars with same h, see Fig. 2(a) and (b), indicating n is strongly intrinsic size-h dependent. For example, n for $\phi = 300$ and 800 nm Cu/Zr pillars with $h = 10$ nm is about 0.3 and 0.325, respectively. As decreasing h from 125 to ~20 nm, n smoothly reduces from ~0.5 down to ~0.4 and then sharply decreases with further reduction in h (see Fig. 2c), similarly to that of Cu[31,32].

On the other hand, the strain hardening rate θ of Cu/Zr pillar with various diameters is determined as the difference between the strength at 0.2% and 2% plastic strain, which is consistent with the θ values at small plastic strains estimated from these fitting curves (see Fig. 2d) by using the strain hardening rate equation, *i.e.*, $\theta = d\sigma/d\varepsilon$. It is found that θ, similarly to n, is still intrinsic rather than extrinsic size-controlled. A maximum $\theta \sim 20$ GPa for Cu/Zr and ~12 GPa for Cu/Cr far greater than that of bulk Cu ~ 2.5 GPa[30,33], is respectively observed at $h \sim 20$ nm, as shown in Fig. 2(d). The inverse layer thickness h (or grain size d) effect reported here has also been observed in Cu films with thickness spanning from 20 to

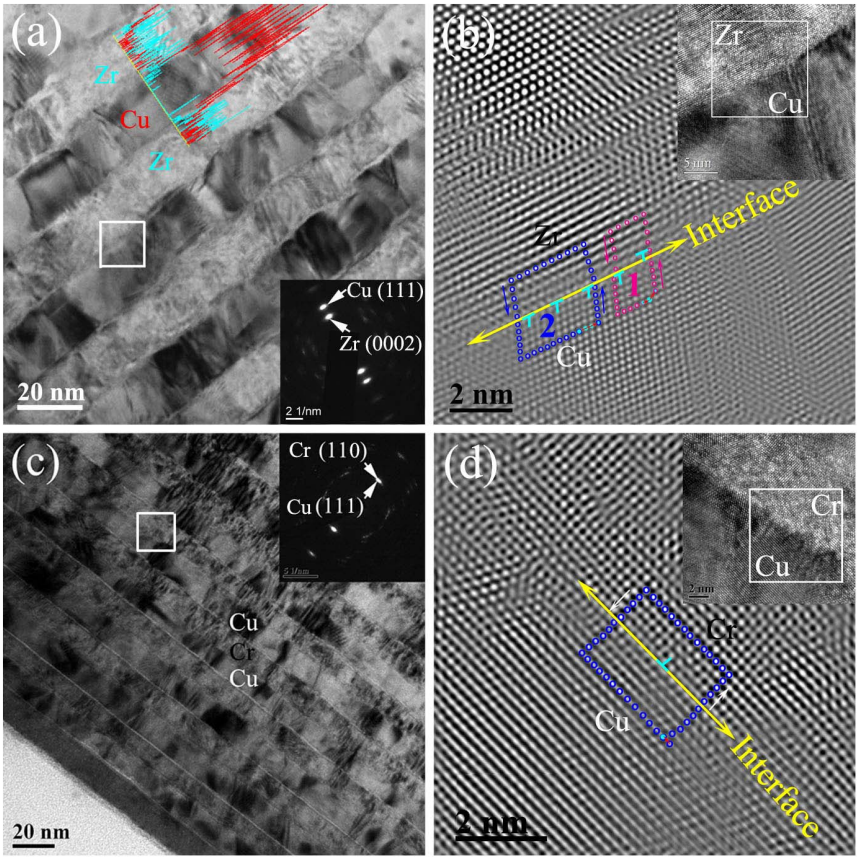

Figure 1 | Bright-field cross-sectional TEM micrographs showing the microstructure of (a) the $h = 20$ nm Cu/Zr multilayers, and (c) the $h = 12.5$ nm Cu/Cr multilayers, respectively. Insets in (a, c) are the corresponding selected area diffraction patterns (SADPs). The line EDX analysis in (a) showing the modulated layer structure without significant intermixing between Cu and Zr. (b) and (d) are the inverse fast Fourier transform (IFFT) HRTEM image of white squared box regions of their insets showing atomic structure of Cu/Zr interface and that of Cu/Cr, respectively. Insets in (b, d) are the HRTEM images typically showing the interface of the corresponding white square boxed area in (a, c). Two Burgers circuit are labeled **1** and **2** in (b), respectively, to determine the Burgers vector of misfit dislocations. A Burgers circuit is drawn in (d) determining the Burgers vector of misfit dislocations as $\boldsymbol{b} = a/2[110]$.

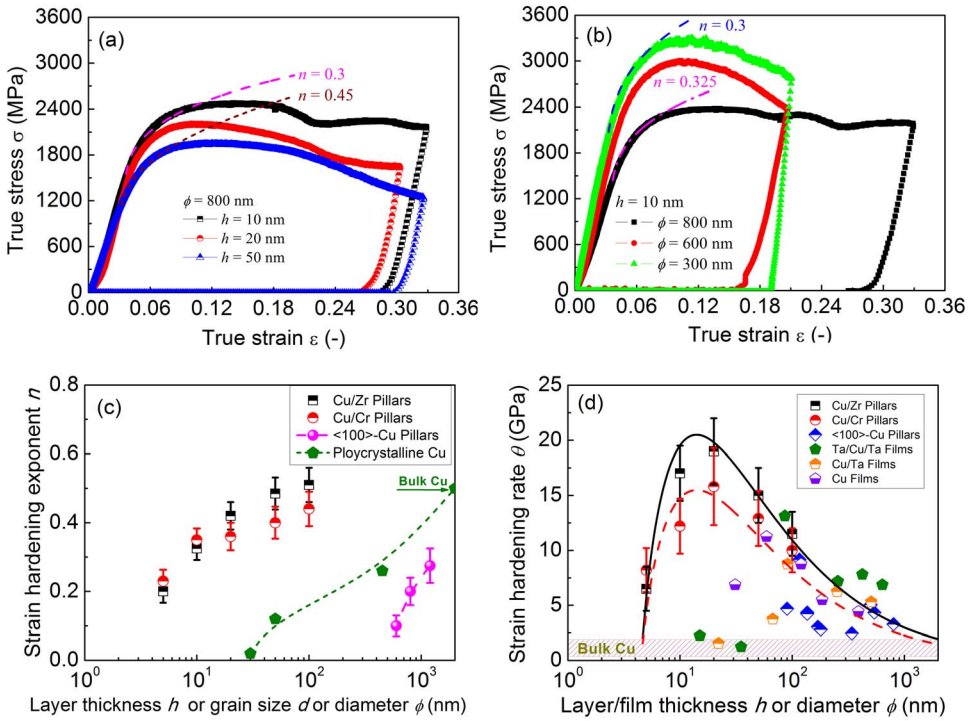

Figure 2 | (a) True stress - strain plots for the $\phi = 800$ nm Cu/Zr micropillars with three different h, and (b) True stress - strain plot for $h = 10$ nm Cu/Zr micropillars with varies ϕ loaded perpendicular to the layer interface. The strain hardening stage is fitted by using power-law strain hardening equation: $\sigma \propto \varepsilon_p^n$. (c) The intrinsic size-controlled strain hardening exponent n as a function of h, compared with that of Cu[31,32] (as a function of grain size d and pillar diameter ϕ). (d) The intrinsic size-controlled strain hardening rate θ of Cu/Zr micropillars as a function of h, compared with that of Cu micropillars[33] and of Cu thin films[34].

800 nm[34]. Moreover, it appears that the Cu/Zr samples have a greater θ than that of Cu/Cr ones at an identical h, which is likely caused by the higher density of misfit dislocations or the larger mismatch strain $\delta \sim 11.2\%$ in Cu/Zr.

Strength of nanolayered micropillars. The intrinsic and extrinsic size effects on strength of the Cu/Zr pillars are studied in comparison. In Fig. 3(a) and (b), the maximum strength σ_{max} is depicted as a function of ϕ at different h for Cu/Zr and Cu/Cr pillars, respectively. It appears that both the σ_{max} of Cu/Zr and Cu/Cr micropillars monotonically increase with decreasing h in the fashion of smaller is stronger. Compare the Cu/Zr samples with the Cu/Cr ones at a given h, it is interesting to find that σ_{max} weakly depends on ϕ when $h > 20$ nm and that α are almost identical within the scatter ($\alpha = 0.06 \pm 0.02$), while σ_{max} strongly depends on ϕ when $h < 20$ nm with $\alpha = 0.3$–0.4 for both Cu/Zr and Cu/Cr samples (see Fig. 3c). Unexpectedly, the critical size of transition from ϕ-independent to ϕ-dependent, *i.e.*, the transition from bulk-like to small-volume materials behavior in the present two types of NMM, is observed at the close intrinsic sizes $h \sim 20$ nm.

Deformation morphologies of nanolayered micropillars. Fig. 4(a, c, e, g) and their insets present SEM/FIB images of $\phi = 600$ nm Cu/Zr micropillars with different h before and after compression (~20–30% strain). After compression, Cu/Zr micropillars with $h > 20$ nm display the homogeneous deformation, *i.e.*, extrusion of Cu in between the hard Zr layers accompanied with barreling, as shown in Fig. 4(a, c). It is demonstrated that the soft phase Cu dominates the plastic deformation, whereas plastically deforming the hard phase Zr is difficult. Moreover, localized interfacial debonding regions are observed, as shown in Fig. 4(b, d). At medium to small scales $h \leq 20$ nm, Cu/Zr micropillars without extrusion of Cu exhibit localized shear banding at great strains shown in Fig. 4(e, g), implying the layers within the shear band have undergone corotation in addition to codeformation of Cu and Zr layers, similarly to $h = 40$ nm-sized Cu/Nb micropillars[10]. Surprisingly, the layered morphology remains intact across the shear band in Fig. 4(f), with no apparent discontinuity (*i.e.*, localized interface crossing in Fig. 4h) as observed in $h = 5$ nm-sized Cu/Nb samples[11]. The same phenomena are observed in other sample sized pillars, as shown in the Supplementary Information for Figures.

In sharp contrast with the Cu/Zr NMM with great $\delta \sim 11.2\%$, the $\phi = 600$ nm Cu/Cr samples with small $\delta \sim 2.3\%$ are more preferred to slip along interfaces with greater extrusion of soft material (Cu) at large scales ≥ 50 nm (see Fig. 5a–d), implying weaker interfaces of Cu/Cr samples[10,21]. Furthermore, no localized interfacial debonding regions is observed, as shown in Fig. 5(b, d). At interim scales, the Cu/Cr micropillars still exhibit extrusion of Cu in between the Cr layers, implying the Cu/Cr samples are less favored to deform by localized shear bands, see Fig. 5(e). Only at the extremely small scale $h = 5$ nm, the Cu/Cr micropillars show the localized shearing by cutting interfaces, see Fig. 5(f). It should be noted that, although the extrinsic size can influence the deformation morphologies of micropillars (e.g. homogeneous shear of the whole pillar vs inhomogeneous shear at the upper part of the pillar), it does not change the intrinsic size-dependent failure mechanisms (e.g. extrusion vs shear banding).

Discussion

Intrinsic size-dependent hardening capability. The strain hardening characteristic is of great importance to structure materials, since the deformation and fracture of these materials are intimately linked to their hardening capability[33], which can be characterized by n and θ. The observed h-dependent strain hardening behavior is reasonable, because it is closely related to the h-dependent dislocation storage capacity[35]. The monotonically reduced n inversely proportional to strength can be ascribed to a greater density of interfacial dislocations in smaller h-sized samples[36]. With regard to

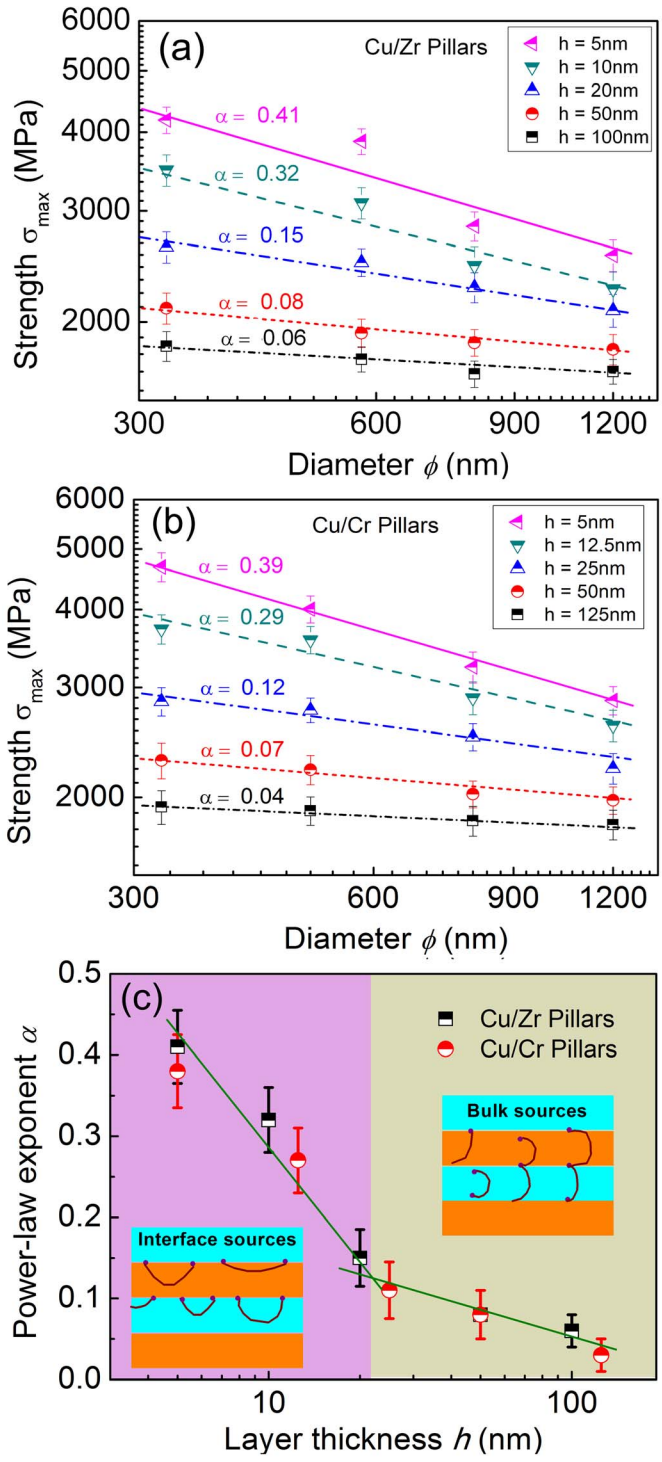

Figure 3 | The maximum strength σ_{max} as a function of ϕ for (a) Cu/Zr and (b) Cu/Cr, respectively. (c) The strength scaling exponent α as a function of h for both Cu/Zr and Cu/Cr.

the maximum θ, it is because that more glide dislocation-interface interactions results in increasing θ with reducing h to a critical value $\sim$ 20 nm, below which the dislocations cross-slip lower the θ, thereby leading to an inverse dependence of θ on h. This was physically and quantitatively explained in terms of reduced dislocations storage rates[35].

Intrinsic and extrinsic sizes driven strength. It is well accepted that the activation of pinned dislocation bulk sources usually requires a lower mechanical stress than that of dislocations emission from surface/interface sources. The dramatic rise in α as a signature of deformation transformed from dislocation interaction processes (bulk-like plasticity) to surface/interface source nucleation/emission (small-scale plasticity) implies that the size-strengthening of Cu/X micropillar is more significant below a transition intrinsic size h = 20 nm[25–29,37]. This is supported by the sharp changes in h-dependent strain hardening capability (n and θ). It is also suggested that the size-dependence itself also manifests a strong size effect; that is to say, the degree of size-strengthening can be very different in distinctly separable h regimes. Numerous findings have explicitly verified that the mechanical response of a nanocrystal is a stronger function of initial microstructure than of size regardless of fabrication methods, which in turn defines the size effect ($\alpha > 0$)[38–40]. In our experiments, the effects of FIB milling on the mechanical properties of all the samples are likely to act in a similar way, and their effects are not considered in the following discussion (More details can be found in Ref. 22). On the other hand, the ϕ-insensitive strength ($\alpha = 0$) can only be found in bulk metals as well as perfect, pristine single crystals.

Because the operation of bulk sources within the layers generally leads to a sample-size independent behavior, *i.e.*, a power law exponent close to zero, similarly to that of bulk polycrystalline metals[41], which indicates the dislocations most likely emit from the Frank-Read type bulk sources at $h > 20$ nm[42]. Also, the absence of intrinsic size h effect on α further verifies that the mechanism responsible for the power law itself is insensitive to h, as the h dependence manifests itself as a deviation from the power law, which has been found in the case of $h < 20$ nm. At small length scale ($h < 20$ nm), a sharp increase in α ($\alpha > 0.2$, sample-size dependent behavior) is simultaneously observed in Cu/Zr and Cu/Cr micropillar as reducing h. This size effect suggests the operation of interface-related dislocation sources because their length can be altered by the reduction in sample size, as it is the case for non-pristine single crystals[25–29] and NC metals[43]. However, at the transition size h = 20 nm, probably on the order of $\rho^{-0.5}$, dislocation interactions would not evolve as they do in samples containing many representative volume elements, since mobile dislocations would have a high probability to exit the sample prior to interacting with other dislocations. In this case, both the volume and interface sources can switch on at this stress level[43]. The fact that the α value of Cu/Zr almost equals to that of Cu/Cr micriopillars at constant h suggests that the soft Cu layers dominate the plastic deformation[44], consistently with the present SEM/FIB observations.

Intrinsic size-dependent deformation modes. Based on these SEM/FIB observations, one can draw a conclusion that there is a strong intrinsic size effect on the deformation modes/failure mechanisms, *i.e.*, extrusion/debonding at great h and shear banding at small h. Above SEM/FIB observations also indicate that two shear banding mechanisms exist at such small-length[10–12]: one is caused by layer rotation, and the other is caused by dislocations cutting cross the interfaces. The rotation and localization of strain within the shear band implies two competing layer-geometry-based mechanisms, with the first being the observed layer thinning, leading to a hardening effect. The second is layer rotation within the band to a softer orientation where the interfaces themselves are more preferred to shear. If the interface plane is weak in shear, the rotation could be sufficient for the resolved shear stress on the interface to facilitate interfacial slip[10]. As such, strain will localize at the interface plane, resulting in the softening exhibited by these materials at high strain (*e.g.* the h = 50 nm Cu/Zr at great strains $\sim$ 20–30%).

To elucidate the intrinsic size dependent deformation modes of nanolayered micropillars with different misfit strains, we consider the dislocation-based pile-up mechanism in a NMM consisting of two metals **A** (*e.g.* Cu) and **B** (*e.g.* X) with the equal h proposed by

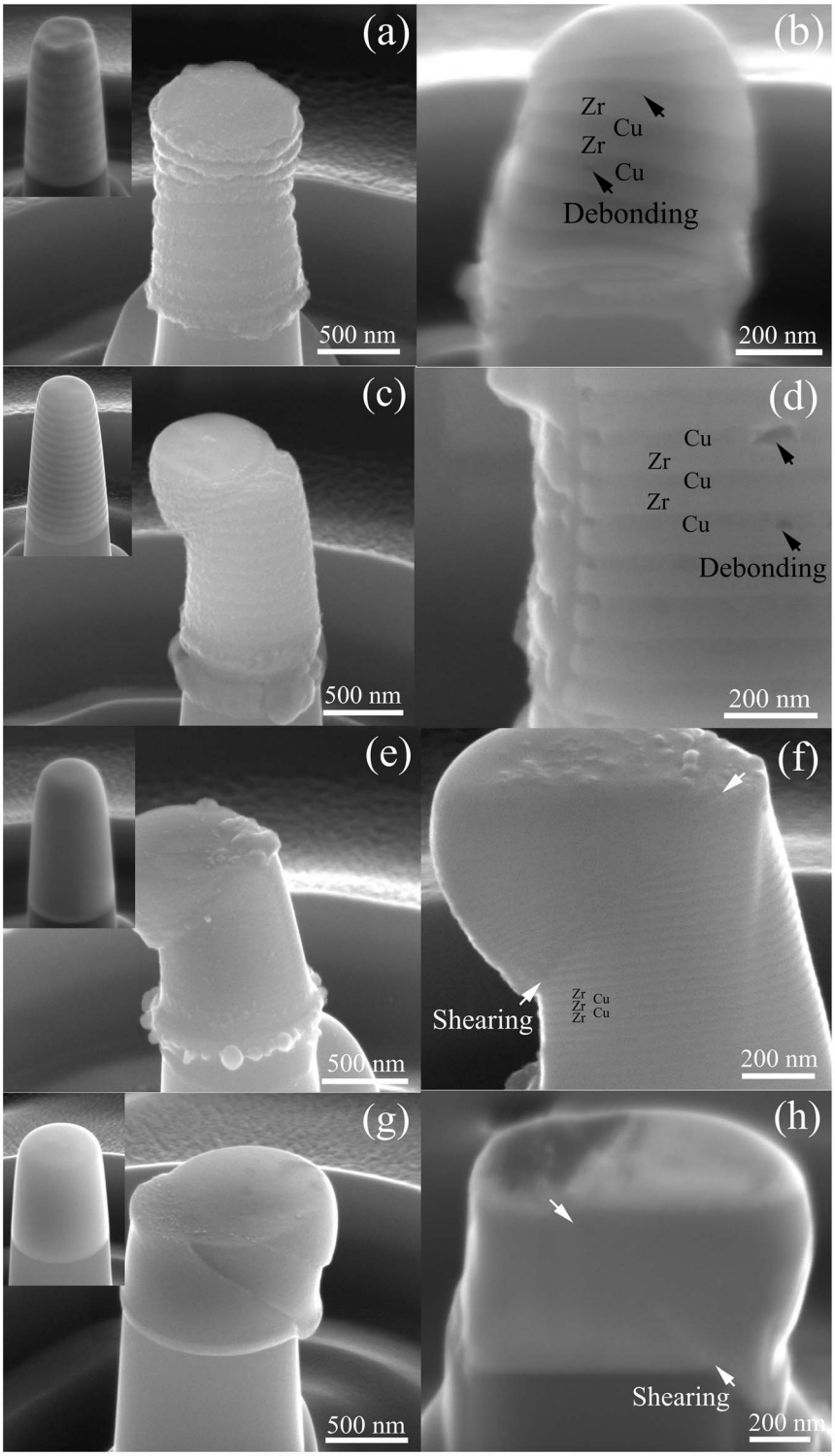

Figure 4 | Typical SEM images (a, c, e, g) of $\phi = 600$ nm nanolayered Cu/Zr micropillars with four different h and their corresponding cross-sectional FIB images (b, d, f, h) after the uniaxial compression tests. (a, b) $h = 100$ nm and (c, d) $h = 50$ nm micropillars barreling of the micropillar (extrusion of Cu), local debonding regions and shear deformation; (e, f) $h = 20$ nm micropillars showing shear deformation and codeformation of constituents layers with intact interfaces; (g, h) $h = 5$ nm micropillars showing highly localized shear banding by interface crossing. Insets are the corresponding SEM images of the as-milled pillars.

Misra et al[45], as shown schematically in Fig. 6(a). Let the initial state be a stress-free multilayer with an array of misfit compensating edge dislocations at the interface to compensate differences in lattice parameters. Because accurately determine the spacing of misfit dislocations (or the mismatch strain) is quite difficult, here we use the theoretical δ to analyze the failure modes of micropillars for simplicity. We further assume that layer **A** has significantly lower yield stress than **B**. Under the applied stress σ, additional dislocations be generated in layer **A**, then pile-up in the interface and transfer load to layer **B** until the stress is sufficient for **B** to begin to flow[45]. At

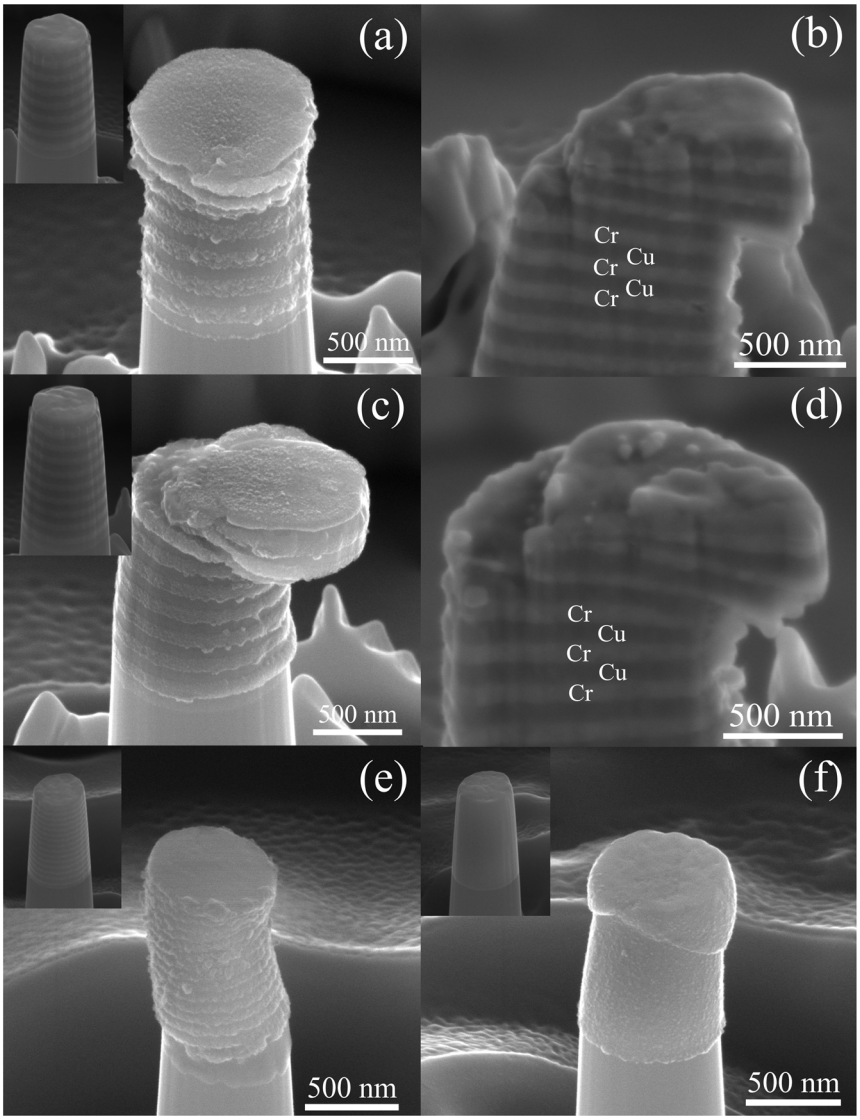

Figure 5 | Typical SEM images (a, c, e, f) of $\phi = 600$ nm nanolayered Cu/Cr micropillars with four different h and their corresponding cross-sectional FIB images (b, d) after the uniaxial compression tests. (a, b) $h = 100$ nm and (c, d) $h = 50$ nm micropillars showing barreling of the micropillar, extrusion of individual Cu layers and interface slipping; (e) $h = 20$ nm micropillars showing barreling of the micropillar, extrusion of individual Cu layers; (f) $h = 5$ nm micropillars showing highly localized shear banding by interface crossing. Insets are the corresponding SEM images of the as-milled pillars.

this stage the structure consists of additional interface dislocations with spacing λ and an effective edge (or screw) dislocation pile-up at a grain boundary in layer **A**. The comparison of the stress components (*i.e.*, shear component, σ_{Shear}, and normal component, σ_{Normal}, of the applied stress due to the edge (or screw) pile-ups with number of dislocations n) in the center of a grain in layer **A** associated with the interface misfit (edge) dislocations barrier, σ_{Edge}, and the interface strength, σ_{IBS}, gives an indication of which controls further flow[45]. Here, the stress components of σ_{Shear} and σ_{Normal} can be derived as[45,46]:

$$\sigma_{Shear} = n\sigma\cos\varphi = \xi\frac{\pi\beta h}{\mu^* b}\sigma^2\cos\varphi = \xi\frac{\pi\beta h}{\mu^* b}\left(\sigma_0 + Kh^{-1/2}\right)^2\cos\varphi, \quad (1)$$

and

$$\sigma_{Normal} = n\sigma\sin\varphi = \xi\frac{\pi\beta h}{\mu^* b}\sigma^2\sin\varphi = \xi\frac{\pi\beta h}{\mu^* b}\left(\sigma_0 + Kh^{-1/2}\right)^2\sin\varphi, \quad (2)$$

Where ξ is a coefficient, $\beta = 1$ for edge and $\beta = (1 - \nu)$ for screw dislocations, where ν is the Poisson ratio for soft phase **A** (~0.343 for Cu); $\mu^* = (\mu_A \cdot \mu_B)/(V_A \cdot \mu_B + V_B \cdot \mu_A)$ is shear modulus of **A**/**B** multilayers, can be estimated by the shear modulus μ_A and volume fraction V_A of **A** layer and that of **B** layer; φ is the angle between the slip plane and the interface ~54.7°, b is the magnitude of the Burgers vector (~0.2556 nm for Cu); the applied stress can be simply expressed as $\sigma = \sigma_0 + Kh^{-1/2}$, where σ_0 is lattice friction stress, and K is the Hall-Petch slope. The interface edge array barrier σ_{Edge}[45] and the interface strength σ_{IBS}[17,19] are given by the following equations, respectively:

$$\sigma_{Edge} = \frac{\mu^* b}{2\lambda(1-\nu)}\coth\left(\frac{\pi h}{2\lambda}\right), \quad (3)$$

and

$$\sigma_{IBS} = M\left[\zeta\mu^*\left(\delta - \frac{b}{2h}\right) + \frac{R\mu_{A/B}\sin\varphi}{8\pi}\right], \quad (4)$$

where ζ is Saada's constant ~0.4; $R = |(\mu_A - \mu_B)/(\mu_A + \mu_B)|$; $\mu_{A/B}$ is the modulus of rigidity of the low-elastic-constant constituent for the

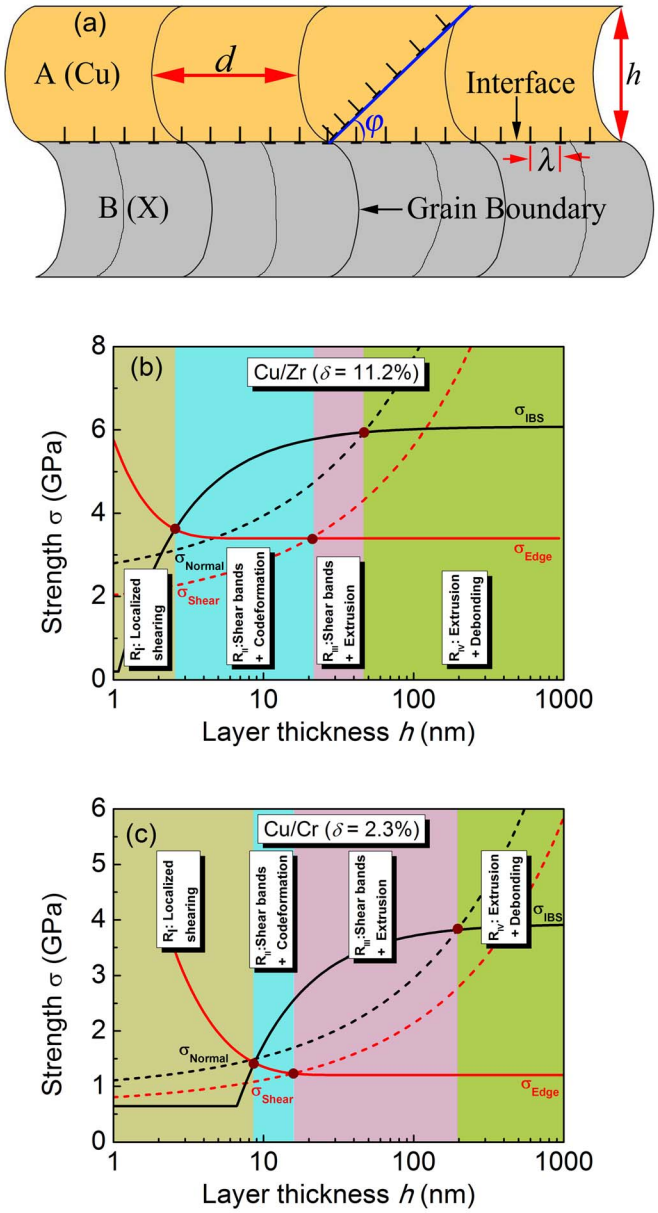

Figure 6 | (a) Schematic of **A**/**B** multilayer with an edge (or screw) dislocation pile-up at a grain boundary in layer **A** and an array of misfit dislocations with edge character at the interface. Deformation mode-maps for different NMM systems with different (b) $\delta \sim 11.2\%$ for Cu/Zr and (c) $\delta \sim 2.3\%$ for Cu/Cr. Four regimes, *i.e.*, R_I: localized shearing, R_{II}: shear bands + codeformation, R_{III}: shear bands + extrusion, and R_{IV}: extrusion + localized debonding, are included in a deformation mode-map.

A/**B** NMM; and other symbols have the same meaning defined before. Note that $\delta = \left(b/2h\right)$ means the interface is fully coherent (without misfit dislocations)[17,19].

Taking $\mu_A = 48.3$ GPa for Cu, $\mu_B = 33$ GPa (for Zr) and $=115.4$ GPa (for Cr), $V_A = V_B = 0.5$, $K = 8.8$ GPa·nm$^{1/2}$ (for Cu/Zr[44]) and 9.8 GPa·nm$^{1/2}$ (for Cu/Cr[47]), $\sigma_0 = 20$ MPa[40], we plotted σ_{Shear}, σ_{Normal}, σ_{Edge}, and σ_{IBS} in Fig. 6(b, c) as a function of h for different NMMs with different δ. It is found that σ_{Shear}, σ_{Normal} and σ_{IBS} increase with increasing h, while σ_{Edge} decreases with increasing h, and there are three crossover points between σ_{IBS} and σ_{Edge}, between σ_{Normal} and σ_{IBS}, and between σ_{Shear} and σ_{Edge} that divide the strength-layer thickness map into four regimes (*i.e.*, R_I, R_{II}, R_{III}, R_{IV}).

In NMMs, dislocations motion (slip *vs* transmission) depends on the two competing effects: the blocking effects of misfit dislocations, σ_{Edge}, and the interfacial strength σ_{IBS}[15,16,21,30]. If $\sigma_{Edge} > \sigma_{IBS}$, dislocations will transmit across the interfaces, while $\sigma_{Edge} < \sigma_{IBS}$ dislocations motion will be limited within isolated Cu layers. Also, whether the Cu/X nanolayered pillars exhibit the extrusion of soft Cu depends on the competition between the σ_{Edge} and the σ_{Shear}, *i.e.*, $\sigma_{Edge} > \sigma_{Shear}$ no extrusion of materials, while $\sigma_{Edge} < \sigma_{Shear}$ the soft Cu can be squeezed out of the micropillars. Therefore, in R_I ($\sigma_{Edge} > \sigma_{Shear}$), $\sigma_{Edge} > \sigma_{IBS}$ indicates that the interfaces cutting mechanism prevails, and the applied stress σ greater than σ_{IBS}, leading to localized shearing via dislocation cutting cross the interfaces[11,12]. This renders the observed macroscopic localized shearing (Fig. 4g, h). In R_{II} ($\sigma_{Edge} > \sigma_{Shear}$), $\sigma_{Normal} < \sigma_{IBS}$ implies that the constituent layers codeform and that the applied stress σ and/or local stress concentrations promotes the rotation of interfaces/layers[10], resulting in the formation of shear bands without extrusion of Cu (Fig. 4e, f). In R_{III} ($\sigma_{Shear} > \sigma_{Edge}$), $\sigma_{Normal} < \sigma_{IBS}$ means that both the extrusion of Cu and interfaces/layers rotation occur simultaneously, inducing the barreling of nanolayered pillars accompanied with shear bands[35]. In R_{IV} ($\sigma_{Shear} > \sigma_{Edge}$), $\sigma_{Normal} > \sigma_{IBS}$ suggests that in addition to the extrusion of Cu (barreling of micropillars), void formation is the main stress relaxation mechanism[48], rendering the localized debonding of interfaces (Fig. 4b, d). The results for Cu/Zr with 11.2% misfit (see Fig. 6b) may be compared with other systems such as Cu/Nb[10,11] where {111} FCC and {110} BCC planes define the misfit strain at the incoherent interface; while the results for Cu/Cr with 2.3% misfit (see Fig. 6c) may be compared with experimental data on Cu/Ni and Cu/Co multilayers. The acceptable discrepancy between the present experimental findings and the theoretical calculations at small h (<10 nm) is likely caused by the change of δ or λ associated with the atomic structure of interface. Furthermore, this model can well explain the h-dependent deformation modes of other systems such as FCC/FCC Al/Pd[24]. Specifically, it is noteworthy from Fig. 6(b, c) that to sustain structural stability (*i.e.*, codeformation) of the nanolayered micropillars, the ideal layer geometry should be a thickness around 20 nm, at which they have the maximum strain hardening capability simultaneously. Additionally, it is suggested that the NMM with smaller δ exhibits greater stain compatibility and is more favorable to achieve fully coherent interfaces.

The development or selection of a material to meet given design requirements generally requires that a compromise be struck between several, usually conflicting, objectives, to balance and optimize a number of metrics of robust performance in the product in which it is used. In this work, we uncovered that in some nanolyayered micropillars composed of alternating soft/hard or ductile/brittle layers such as Cu/Zr and Cu/Cr, their strength increases monotonically with decreasing intrinsic size h, displaying the transition from bulk-like to small-scale materials behavior, while the strain hardening rate, contrary to the popular belief, exhibit an inverse h-dependence at a critical $h \sim 20$ nm. The intrinsic size h-dependent failure modes transited from extrusion/debonding to localized interface cutting is quantitatively explained by a dislocation-based model. These results will provide impetus for microstructure sensitive design of such nanolayered materials in technological applications because their sizes and properties are highly tunable by controlling the layer geometry and the interface characteristics.

Methods

Multilayer synthesis and microstructure characterization. The Si-supported Cu/X (X = Zr, Cr) NMM with total thickness ~2 μm were respectively prepared by using direct current (*dc.*) magnetron sputtering at room temperature. The thickness of Cu layer equals that of X layer and covers a wide range spanning from ~5 to ~125 nm. High resolution transmission electron microscopy (HR-TEM)

and energy dispersive X-ray (EDX) analyses to identify the elemental composition and the interface integrity of the specimens were performed on a JEOL-2100F TEM. More details about the synthesis and the internal features of Cu/X NMM can be found in literatures[22,44].

Mechanical test of nanolayered micropillars. The Cu/X micropillars with the layer interfaces perpendicular to the cylinder axis were fabricated from the as-deposited NMMs using a Helios Nano Lab 600i dual-beam focused ion beam (FIB) system. The diameter of the pillar (ϕ) was chosen to be from 300 to 1200 nm to restrict the pillar geometry in order to avoid buckling of the sample during subsequent uniaxial microcompression tests. The taper angles (ψ) of the pillars were measured between 2° to 4°. All the pillars were then uniaxially compressed in a Hysitron Ti 950 with a 10 μm side-flat quadrilateral cross-section diamond indenter at constant strain rate of 2×10^{-4} s^{-1} up to ~20–30% strain. True stress-strain curves were calculated using a constant volume and homogeneous deformation assumption model to characterize the deformation behaviors[22,40]. More details about the micropillars preparation procedures, testing methods and true stress-strain curve calculation procedure can be found in Supplementary Information for Methods.

1. Fullwood, D. T., Niezgoda, S. R., Adams, B. L. & Kalidindi, S. R. Microstructure sensitive design for performance optimization. *Prog. Mater. Sci.* **55**, 477–562 (2010).
2. Zhu, T. & Li, J. Ultra-strength materials. *Prog. Mater. Sci.* **55**, 710–757 (2010).
3. Zheng, S. *et al*. High-strength and thermally stable bulk nanolayered composites due to twin-induced interfaces. *Nat Commun* **4**, 1696 (2013).
4. Demkowicz, M. J., Misra, A. & Caro, A. The role of interface structure in controlling high helium concentrations. *Curr. Opin. Solid State Mater. Sci.* **16**, 101–108 (2012).
5. Kim, J. Y., Jang, D. C. & Greer, J. R. Nanolaminates Utilizing Size-Dependent Homogeneous Plasticity of Metallic Glasses. *Adv. Funct. Mater.* **21**, 4550–4554 (2011).
6. Zhang, J. Y. *et al*. An easy way to prepare layered nanoplatelets: Fragment of nanostructured multilayers. *J. Appl. Phys.* **111**, 113519 (2012).
7. Wang, Y. M., Li, J., Hamza, A. V. & Barbee, J. T. W. Ductile crystalline-amorphous nanolaminates. *Proc. Natl. Acad. Sci. USA* **104**, 11155–11160 (2007).
8. Bakonyi, I. & Péter, L. Electrodeposited multilayer films with giant magnetoresistance (GMR): Progress and problems. *Prog. Mater. Sci.* **55**, 107–245 (2010).
9. Was, G. S. & Foecke, T. Deformation and fracture in microlaminates. *Thin Solid Films* **286**, 1–31 (1996).
10. Mara, N. A., Bhattacharyya, D., Hirth, J. P., Dickerson, P. & Misra, A. Mechanism for shear banding in nanolayered composites. *Appl. Phy. Lett.* **97**, 021909 (2010).
11. Mara, N. A., Bhattacharyya, D., Dickerson, P., Hoagland, R. G. & Misra, A. Deformability of ultrahigh strength 5 nm Cu/Nb nanolayered composites. *Appl. Phy. Lett.* **92**, 231901 (2008).
12. Han, S. M., Phillips, M. A. & Nix, W. D. Study of strain softening behavior of Al-Al3Sc multilayers using microcompression testing. *Acta Mater.* **57**, 4473–4490 (2009).
13. Zhang, J. Y. *et al*. Length scale dependent deformation behavior of nanolayered Cu/Zr micropillars. *Acta Mater.* **60**, 1610–1622 (2012).
14. Knorr, I., Cordero, N. M., Lilleodden, E. T. & Volkert, C. A. Mechanical behavior of nanoscale Cu/PdSi multilayers. *Acta Mater.* **61**, 4984–4995 (2013).
15. Misra, A., Hirth, J. P. & Hoagland, R. G. Length-scale-dependent deformation mechanisms in incoherent metallic multilayered composites. *Acta Mater.* **53**, 4817–4824 (2005).
16. Anderson, P. M., Foecke, T. & Hazzledine, P. M. Dislocation-based Deformation Mechanisms in Metallic Nanolaminates. *MRS Bull.* **24**, 27–33 (1999).
17. Liu, Y. *et al*. Stacking fault and partial dislocation dominated strengthening mechanisms in highly textured Cu/Co multilayers. *Inter. J.Plasticity* **49**, 152–163 (2013).
18. Hoagland, R. G., Kurtz, R. J. & Henager, C. H. Slip resistance of interfaces and the strength of metallic multilayer composites. *Scripta Mater.* **50**, 775–779 (2004).
19. Rao, S. I. & Hazzledine, P. M. Atomistic simulations of dislocation-interface interactions in the Cu-Ni multilayer system. *Phil. Mag. A* **80**, 2011–2040 (2000).
20. Zbib, H. M., Overman, C. T., Akasheh, F. & Bahr, D. Analysis of plastic deformation in nanoscale metallic multilayers with coherent and incoherent interfaces. *Inter. J. Plasticity* **27**, 1618–1639 (2011).
21. Wang, J. & Misra, A. An overview of interface-dominated deformation mechanisms in metallic multilayers. *Curr. Opin. Solid State Mater. Sci.* **15**, 20–28 (2011).
22. Zhang, J. Y., Liu, G. & Sun, J. Comparisons between homogeneous boundaries and heterophase interfaces in plastic deformation: Nanostructured Cu micropillars vs. nanolayered Cu-based micropillars. *Acta Mater.* **61**, 6868–6881 (2013).
23. Yan, J. W., Zhu, X. F., Yang, B. & Zhang, G. P. Shear Stress-Driven Refreshing Capability of Plastic Deformation in Nanolayered Metals. *Phy. Rev. Lett.* **110**, 155502 (2013).
24. Dayal, P., Quadir, M. Z., Kong, C., Savvides, N. & Hoffman, M. Transition from dislocation controlled plasticity to grain boundary mediated shear in nanolayered aluminum/palladium thin films. *Thin Solid Films* **519**, 3213–3220 (2011).
25. Dehm, G. Miniaturized single-crystalline fcc metals deformed in tension: New insights in size-dependent plasticity. *Prog. Mater. Sci.* **54**, 664–688 (2009).
26. Kraft, O., Gruber, P. A., Mönig, R. & Weygand, D. Plasticity in Confined Dimensions. *Annu. Rev. Mater. Res.* **40**, 293–317 (2010).
27. Uchic, M. D., Shade, P. A. & Dimiduk, D. M. Plasticity of Micrometer-Scale Single Crystals in Compression. *Annu. Rev. Mater. Res.* **39**, 361–386 (2009).
28. Greer, J. R. & De Hosson, J. T. M. Plasticity in small-sized metallic systems: Intrinsic versus extrinsic size effect. *Prog. Mater. Sci.* **56**, 654–724 (2011).
29. Fertig, R. S. & Baker, S. P. Simulation of dislocations and strength in thin films: A review. *Prog. Mater. Sci.* **54**, 874–908 (2009).
30. Misra, A., Zhang, X., Hammon, D. & Hoagland, R. G. Work hardening in rolled nanolayered metallic composites. *Acta Mater.* **53**, 221–226 (2005).
31. Lu, L., Chen, X., Huang, X. & Lu, K. Revealing the maximum strength in nanotwinned copper. *Science* **323**, 607–610 (2009).
32. Zhang, J. Y. *et al*. Emergence of external size effects in the bulk-scale polycrystal to small-scale single-crystal transition: A maximum in the strength and strain-rate sensitivity of multicrystalline Cu micropillars. *Acta Mater.*, doi:http://dx.doi.org/10.1016/j.actamat.2013.11.018.
33. Kiener, D. & Minor, A. M. Source-controlled yield and hardening of Cu(1 0 0) studied by in situ transmission electron microscopy. *Acta Mater.* **59**, 1328–1337 (2011).
34. Gruber, P. A. *et al*. Size effects on yield strength and strain hardening for ultra-thin Cu films with and without passivation: A study by synchrotron and bulge test techniques. *Acta Mater.* **56**, 2318–2335 (2008).
35. Lei, S. Y. *et al*. Intrinsic size-controlled strain hardening behavior of nanolayered Cu/Zr micropillars. *Scripta Mater.* **66**, 706–709 (2012).
36. Csiszár, G., Misrab, A. & Ungár, T. Burgers vector types and the dislocation structures in sputter-deposited Cu–Nb multilayers. *Mater. Sci. Eng. A* **528**, 6887–6895 (2011).
37. Kiener, D. & Minor, A. M. Source Truncation and Exhaustion: Insights from Quantitative in situ TEM Tensile Testing. *Nano Lett.* **11**, 3816–3820 (2011).
38. Bei, H., Shim, S., Pharr, G. M. & George, E. P. Effects of pre-strain on the compressive stress-strain response of Mo-alloy single-crystal micropillars. *Acta Mater.* **56**, 4762–4770 (2008).
39. Jennings, A. T., Burek, M. J. & Greer, J. R. Microstructure versus Size: Mechanical Properties of Electroplated Single Crystalline Cu Nanopillars. *Phys. Rev. Lett.* **104**, 135503 (2010).
40. Zhang, J. Y., Liu, G. & Sun, J. Strain rate effects on the mechanical response in multi- and single-crystalline Cu micropillars: Grain boundary effects. *Inter. J. Plasticity* **50**, 1–17.
41. Dao, M., Lu, L., Asaro, R. J., De Hosson, J. T. M. & Ma, E. Toward a quantitative understanding of mechanical behavior of nanocrystalline metals. *Acta Mater.* **55**, 4041–4065 (2007).
42. Beanland, R. Multiplication of misfit dislocations in epitaxial layers. *J. Appl. Phys.* **72**, 4031 (1992).
43. Rinaldi, A., Peralta, P., Friesen, C. & Sieradzki, K. Sample-size effects in the yield behavior of nanocrystalline nickel. *Acta Mater.* **56**, 511–517 (2008).
44. Zhang, J. Y. *et al*. Mechanical properties of crystalline Cu/Zr and crystal–amorphous Cu/Cu–Zr multilayers. *Mater. Sci.Eng. A* **552**, 392–398 (2012).
45. Misra, A., Verdier, M., Kung, H., Embury, J. D. & Hirth, J. P. Deformation mechanism maps for polycrystalline metallic multilayers. *Scripta Mater.* **41**, 973–979 (1999).
46. Courtney, T. H. *Mechanical behavior of materials. Long Grove: Waveland Press* (2000).
47. Misra, A. *et al*. Structure and mechanical properties of Cu-X (X = Nb,Cr,Ni) nanolayered composites. *Scripta Mater.* **39**, 555–560 (1998).
48. Zhang, J., Zhang, J. Y., Liu, G., Zhao, Y. & Sun, J. Competition between dislocation nucleation and void formation as the stress relaxation mechanism in passivated Cu interconnects. *Thin Solid Films* **517**, 2936–2940 (2009).

Acknowledgments

This work was supported by the National Natural Science Foundation of China (Grant Nos. 51321003, 51322104, 51201123), the 973 Program of China (Grant No. 2010CB631003), and the 111 Project of China (B06025). GL thanks the support from Fundamental Research Funds for the Central Universities and the Tengfei Scholar project. JYZ thanks China Postdoctoral Science Foundation (2012M521765) and Shaanxi Province Postdoctoral Scientific Research Projects for part of financial support. Access to the nanoindentation equipments in CAMP-Nano is also acknowledged.

Author contributions

J.S. designed the project and guided the research; J.Y.Z., J.L. and X.Q.L. carried out the experiments; J.Y.Z. analyzed the data and constructed the model; J.Y.Z. and G.L. wrote the paper. All authors contributed to the discussions.

Additional information

Supplementary information accompanies this paper at http://www.nature.com/scientificreports

Competing financial interests: The authors declare no competing financial interests.

How to cite this article: Zhang, J.Y., Li, J., Liang, X.Q., Liu, G. & Sun, J. Achieving optimum mechanical performance in metallic nanolayered Cu/X (X = Zr, Cr) micropillars. *Sci. Rep.* **4**, 4205; DOI:10.1038/srep04205 (2014).